technologies

MDPI

Article

Oil Capture Mechanism and Structural Optimization of Under-Race Lubrication Oil Scoop for High-Speed Bearings

Xiaozhou Hu *, Kang Duan and Bingkun Han

State Key Laboratory of High Performance Complex Manufacturing, School of Mechanical and Electrical Engineering, Central South University, Changsha 410083, China; 243711035@csu.edu.cn (K.D.)
* Correspondence: huxiaozhou@csu.edu.cn; Tel.: +86-13755111783

Abstract

The lubrication of high-speed bearings in variable-speed transmission systems is typically achieved through radial under-race lubrication devices, where the performance of the oil capture section significantly affects the overall lubrication performance. To improve the oil capture performance of radial under-race lubrication devices, this study analyzed the flow mechanism of lubricating oil in the under-race oil capture section to investigate the main factors influencing the oil capture performance. Based on the bearing cavity structure of a specific high-speed bearing, a preliminary design of the oil scoop was conducted. A numerical model of the flow field in the radial under-race lubrication oil capture section was established using CFD methods. Simulations were performed to study the influence patterns of these factors on the oil capture efficiency of the scoop, followed by preliminary optimization of the oil scoop. Through visualization analysis, the main causes of lubricating oil loss were identified, and further optimization of the scoop structure was carried out, significantly improving the oil capture efficiency of the scoop. An oil scoop performance test bench was designed and constructed, and experiments were conducted. The experimental results showed good agreement with the simulation results.

Keywords: under-race lubrication; oil scoop; oil capture efficiency; structural optimization

1. Introduction

High-speed bearings are widely used in aerospace and other fields, providing essential support and connection for variable-speed transmission systems such as aero engines, turbines, and gearboxes. Insufficient lubrication of high-speed bearings can impair the operation of the entire transmission system and may even lead to safety incidents. Since traditional lubrication methods fail to provide adequate lubrication under high-speed conditions, high-speed bearings are typically lubricated using oil jet lubrication or under-race lubrication [1].

There are two methods of under-race lubrication, as shown in Figure 1. The first involves creating an oil delivery channel along the central axis of the shaft where the bearing is mounted to directly achieve under-race lubrication, also known as axial under-race lubrication. The second method utilizes nozzles as the oil source, employing a bearing lubrication device to achieve under-race lubrication while only requiring an under-race lubrication channel on the bearing inner ring, known as radial under-race lubrication. The main shaft inside a variable-speed transmission system must bear torque and bending moments during operation, demanding high load-bearing capacity. Compared to the first

Check for updates

Academic Editor: Juan Gabriel Avina-Cervantes

Received: 7 June 2026
Revised: 2 July 2026
Accepted: 7 July 2026
Published: 10 July 2026

Copyright: © 2026 by the authors. Licensee MDPI, Basel, Switzerland. This article is an open access article distributed under the terms and conditions of the Creative Commons Attribution (CC BY) license.

method, the second approach helps enhance the load-bearing capacity of the shaft. Overall, the second method is more suitable for variable-speed transmission systems.

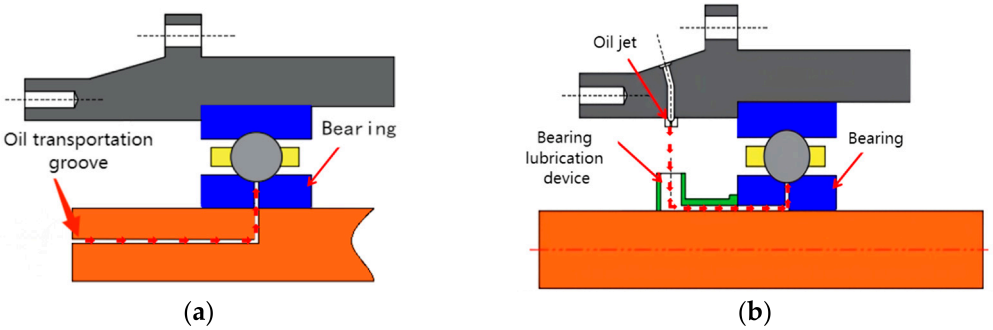


Figure 1. Two implementations of under-race lubrication ((**a**) under-race lubrication of the shaft axis position; (**b**) under-race lubrication by the nozzle).

Many scholars have conducted extensive exploration targeting the lubrication effectiveness of under-race lubrication, obtaining numerous practical conclusions. Nakamura et al. [2] modeled the annular gap between the bearing inner ring and cage during under-race lubrication and performed numerical simulations of the two-phase flow field in this region to study the differences between circumferentially distributed radial oil supply holes and discrete radial oil supply holes in lubricating bearings. Adeniyi et al. [3] investigated the oil distribution between the cage and inner ring when using under-race oil supply holes.

Bao et al. [4,5] employed the Coupled Level Set and Volume of Fluid method to track the oil–air two-phase flow field inside bearings, finding that at sufficiently high speeds, lubricant concentrates at the outer ring due to centrifugal force; without considering the rotation of rollers, the fluid flow direction around rollers approximates the rotational direction with continuously increasing velocity. Jiang et al. [6] examined how inner/outer ring speeds, inlet flow rate, oil temperature, and radial inlet structure affect oil distribution in ball bearings, discovering an optimal outer ring speed for best lubrication, with oil diffusion decreasing sequentially from outer ring to cage, balls, and inner ring, and optimized oil hole configuration based on average oil volume fraction. Lyu et al. [7] studied fluid behavior in under-race lubricated ball bearings, developed an oil volume fraction prediction model quantifying effects of bearing speed, oil flow rate, viscosity, and density, and established a predictive formula for average oil volume fraction in bearing ring cavities based on simulation results. Gao et al. [8,9] investigated oil distribution characteristics in aero-engine roller bearings, finding oil struggles to flow through gaps between cage pockets and rollers, with higher viscosity worsening this effect; they analyzed lubricant resistance on rotating spherical elements in high-speed ball bearings, developed both simulation and experimental models for multi-sphere flow with separator plates (errors < 10%), and created a ball resistance prediction formula.

Some researchers focused on radial under-race lubrication device design. Kenneth et al. [10,11] developed an integrated under-race oil supply device for a main shaft, effectively solving leakage issues from traditional oil capture structures, and further proposed a bidirectional oil supply radial scoop comprising four blades and oil channels, where circumferential position adjustment enables oil distribution control. Joseph [12] introduced a radial oil capture method using two annular bodies jets that enter the first annular space then flow into the second by inertia before reaching the inner ring via centrifugal force. Stephen [13] designed a radial oil capture shaft without blades, using axially distributed grooves where jets directly deposit oil at acute angles to the shaft end face, with collected oil flowing through reservoirs to bearings.

Radial under-race lubrication devices consist of oil capture and delivery sections, whose performances determine oil capture efficiency and delivery stability. Many studies have investigated capture efficiency: Paleo et al. [14] experimentally examined the factors affecting scoop efficiency across three supply devices with different jet angles and velocity ratios. Ya et al. [15] numerically evaluated capture efficiency under different conditions. Jiang et al. [16–19] established relationships between the liquid–gas momentum ratio and jet breakup location, derived pre-breakup trajectory equations to optimize nozzle position, studied the effects of jet velocity, oil temperature, and single- and dual-nozzle configurations on efficiency, and further analyzed the influence of hole spacing. Hou et al. [20] investigated how orifice diameter affects efficiency and flow velocity and determined an appropriate diameter range. Le et al. [21] combined experiments and simulations to study two-phase flow characteristics and developed a corrected discharge-coefficient formula showing that adjusted pressure differentials and jet angles can reduce oil loss. Zhang et al. [22] found that reducing the scoop radius difference improves efficiency and quantitatively evaluated the influence of design parameters through global sensitivity analysis, with prediction errors below 4%.

Some researchers focused on improving oil scoop structures: Jonathan et al. [23] proposed curved-surface blades based on optimal jet-blade relative velocity. Kruisbrink et al. [24] characterized oil splash/capture conditions using jet angle/velocity ratio, introducing new analytical methods for jet-blade positioning. Qin et al. [25] designed a radial scoop where the synthetic velocity direction always aligns with inlet curve tangents, guiding oil into channels at any collision point.

In addition, Milojević et al. [26] showed that lubrication-related structural improvement can effectively alleviate friction and wear and improve operational performance, while Gajević et al. [27] demonstrated that optimization strategies combining Taguchi, gray relational analysis, and TOPSIS can effectively enhance tribological characteristics. These studies further highlight the engineering importance of lubrication-related structural design and optimization.

Although previous studies have substantially advanced the understanding of radial under-race lubrication, most of them focused on the effects of operating parameters, nozzle arrangements, or overall geometric parameters on oil capture efficiency. In contrast, the present study aims to connect mechanism analysis with structural optimization. First, the oil capture process is analyzed theoretically from the perspectives of jet cutting, flow on the inner and outer blade surfaces, and the geometric relation governing the scoop outer profile. Second, CFD simulations are used not only to evaluate efficiency trends but also to visualize the oil-loss mechanism during capture. Third, based on the identified loss mechanism, an optimized oil scoop with subdivided blades and an additional drainage groove is proposed. Finally, the numerical method is validated experimentally. Therefore, the novelty of this work lies in integrating mechanism-based analysis, CFD-guided structural optimization, and experimental validation for the design of radial under-race oil scoops.

2. Oil Capture Mechanism Analysis

Figure 2 shows the internal structure of the bearing cavity in a specific variable-speed transmission system of a helicopter and the positioning of the radial under-race lubrication device. The device is located between the two bearings. It collects lubricating oil sprayed by vertical nozzles through oil blades and then delivers the oil to the interior of the bearings via an oil delivery structure, achieving lubrication for the high-speed bearings.

The working principle of the radial oil blades involves the rotating blades' leading edges cutting through the lubricant jet. The severed lubricant flows along the blades' inner surfaces into the oil delivery channels under inertial force. During this process, both the

mass of the cut lubricant and whether this portion of lubricant escapes from the capture cavity significantly impact the oil capture efficiency of the radial blades. Therefore, detailed analysis of these two aspects of lubricant flow behavior is required.

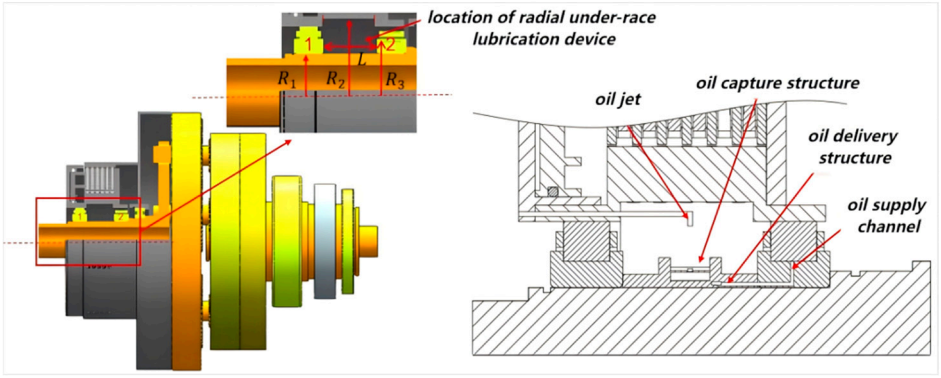


Figure 2. Schematic diagram of the internal structure of variable-speed transmission system.

The basic structure of a typical oil scoop is shown in Figure 3. The geometric relation of the outer surface curve of the oil scoop is shown in Figure 4.

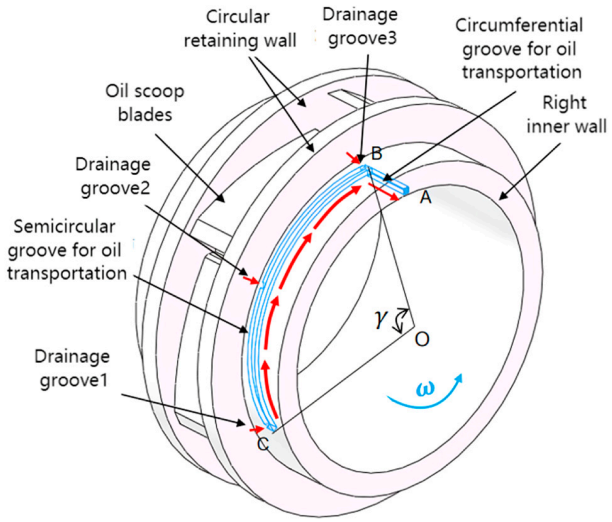


Figure 3. Structural diagram of a typical oil scoop.

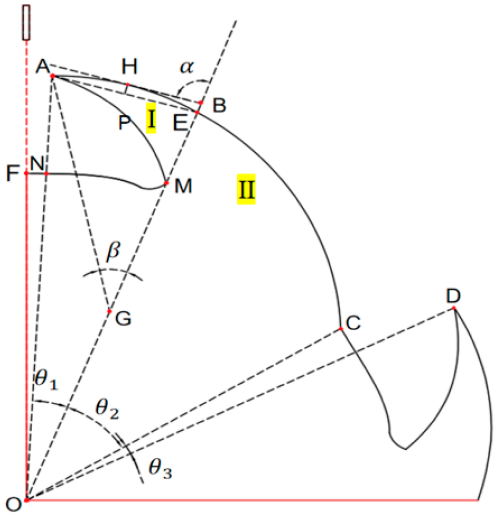


Figure 4. Geometric relation of the outer surface curve of the oil scoop.

In Figure 4, regions I and II denote the jet-cutting part and the flow-guiding part of the scoop outer surface, respectively, while the labeled points are geometric construction points used to define the outer surface curve.

Due to the scoop's high-speed rotation, the lubricant jet entering this rotating zone becomes susceptible to air resistance-induced deflection. The kinetic energy equation reveals that larger nozzle diameters increase both flow rate and kinetic energy at constant velocity, thereby enhancing the jet's anti-deflection capability. Furthermore, excessive nozzle-to-scoop distance may cause jet front breakup and atomization. For analytical simplicity, subsequent studies disregard jet deflection, breakup, and atomization effects, treating the jet as a uniform cylindrical flow perpendicular to the axis.

2.1. Analysis of Oil Capture at the Leading Edge of Oil Scoop

Figure 5 illustrates the process from an arbitrary initial state to the first cutting of the lubricant jet by the oil scoop. The nozzle ejects lubricant at a velocity of V_{oil}, with the jet direction perpendicular to the axis. Since the influence of air resistance is neglected, the velocity and direction of the jet remain unchanged before colliding with the scoop wall. In the initial state, the oil scoop can be positioned at any location and rotates counterclockwise at an angular velocity ω of over time.

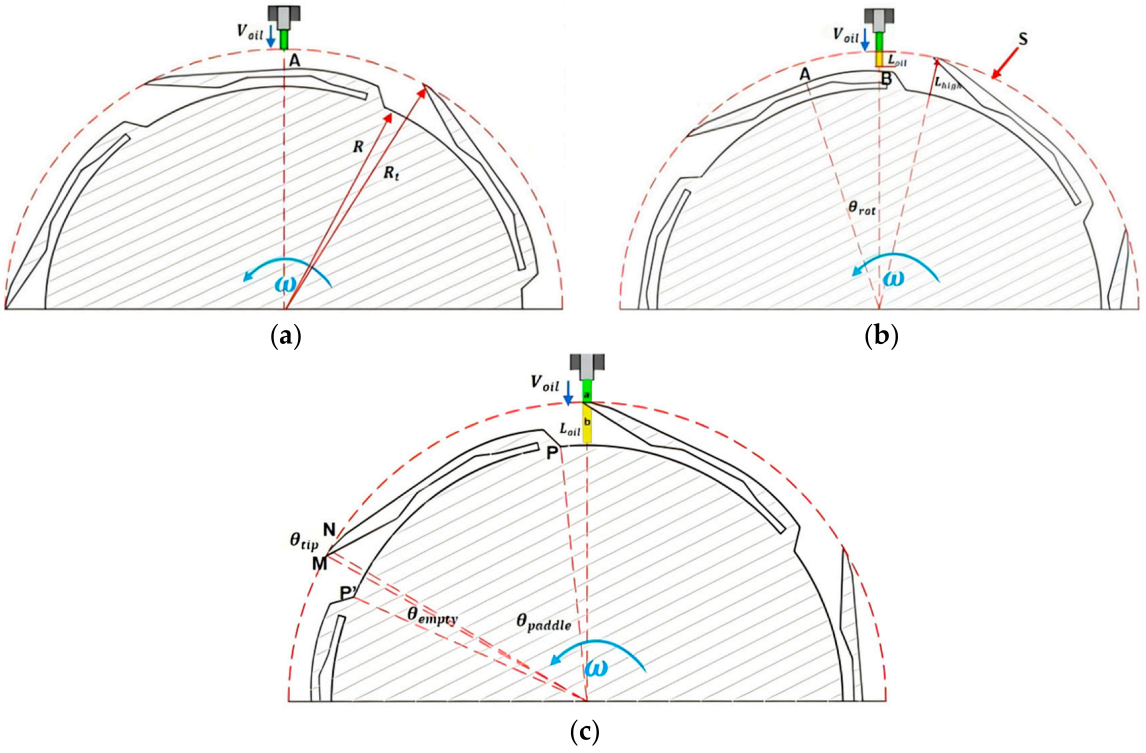


Figure 5. Analysis of jet cutting state by oil scoop. ((**a**) Initial relative position between oil scoop and lubricant jet; (**b**) relative motion relationship when jet enters the capture region without being cut; (**c**) state of oil scoop leading edge first cutting the lubricant jet).

Figure 5b shows the relative motion relationship between the oil scoop and the lubricant jet. In the figure, the jet does not collide with the outer surface. However, if the jet velocity is too high or the scoop rotation speed is too low, the lubricant jet may collide with the outer surface of the scoop before being cut, generating splashed plumes under the impact force and causing lubricant to escape the capture region, thereby reducing the oil capture efficiency of the scoop.

Here, S represents the circle formed by the highest points on the outer surface of the oil scoop. The area inside this circle is the capture region. L_{oil} denotes the length of the jet

entering the capture region (yellow area in the figure), while L_{high} represents the maximum length of the jet that can be cut. So L_{oil} can be expressed as:

$$L_{oil} = \frac{\theta_{rot} V_{oil}}{\omega} \tag{1}$$

In Equation (1), θ_{rot} represents the rotation angle when the scoop reaches the position shown in Figure 5b; V_{oil} denotes the oil injection velocity of the nozzle; ω indicates the angular velocity of the main shaft rotation.

As shown in Figure 5b, the magnitude of L_{high} is related to the distance between the highest point on the outer surface of the oil scoop and the inner wall of the oil capture structure, while θ_{rot} decreases as the number of blades increases. According to Equation (1), increasing the number of blades, raising the rotational speed of the main shaft, or decreasing the nozzle velocity will all result in a reduction in the jet length L_{oil} within the capture region. When $L_{high} - L_{oil} \geq 0$, the lubricant jet can avoid collision with the outer wall of the scoop, preventing oil waste and improving the oil capture efficiency of the radial oil blades.

It should be noted that possible near-contact interaction between the scoop leading edge and the inner wall of the oil capture structure may introduce additional friction and mechanical loss. However, the present study focuses primarily on the oil capture process and lubrication performance, and this contribution is therefore not quantified separately.

In the narrow-gap region between the scoop leading edge and the inner wall of the oil capture structure, local temperature rise may affect lubricant properties and flow behavior. In the present analysis, however, the lubricant is treated as having constant properties within the investigated operating range so that the main oil capture mechanism can be analyzed more clearly.

As illustrated in Figure 5c, over time, the leading edge of the oil scoop makes initial contact with the lubricant jet, dividing the jet cylinder into two parts (a and b). Assuming no oil spills when flowing along the inner wall of the scoop, the oil mass M_b of jet cylinder b can be regarded as the captured oil mass of this oil scoop. M_b can be expressed as:

$$M_b = \rho \frac{\pi d_{jet}^2}{4} L_{oil} \tag{2}$$

where ρ is the lubricant density.

If there is no contact between the oil jet and the outer wall of the scoop before the scoop tip contacts the lubricating oil jet, L_{oil} can be expressed as:

$$L_{oil} = (\theta_{paddle} + \theta_{empty} - \theta_{tip}) \frac{V_{oil}}{\omega} \tag{3}$$

In Equation (3), θ_{paddle} represents the angle between the scoop tip M and end point P of the oil scoop; θ_{empty} denotes the angle between the scoop end point P' and tip M; θ_{tip} indicates the angle at the tip of the oil scoop.

Therefore, the oil mass M_b of jet cylinder b can be expressed as:

$$M_b = \rho \frac{\pi d_{jet}^2}{4} (\theta_{padde} + \theta_{empty} - \theta_{tip}) \frac{V_{oil}}{\omega} \tag{4}$$

If contact occurs between the oil jet and the outer scoop wall before the scoop tip contacts the lubricating oil jet, L_{oil} can be directly expressed as:

$$L_{oil} = L_{high} - R_t - R \tag{5}$$

Under these conditions, the oil mass M_b of jet cylinder b can be expressed as:

$$M_b = \rho \frac{\pi d_{jet}^2}{4} (R_t - R) \tag{6}$$

Assuming all oil jets cut by the scoop tip flow into the next stage without spillage or splashing, Equation (4) indicates that when no contact occurs between the oil jet and outer scoop wall before the scoop tip contacts the lubricating oil jet, the main shaft's rotational speed, scoop structure, length, quantity, injection velocity, and nozzle diameter will all affect the single scoop's oil capture mass. Equation (6) shows that when contact exists between the oil jet and outer scoop wall before the scoop tip contacts the lubricating oil jet, the nozzle diameter, maximum radius of the scoop's outer surface, and inner ring radius of the capture device significantly influence the scoop's oil capture mass.

Analysis of the oil scoop reveals that when the tip of Scoop I first contacts the oil jet just as the jet reaches the connecting inner ring of the scoop, the capture efficiency reaches 100% and the single scoop achieves maximum oil capture mass. Therefore, it can be concluded that

$$\frac{R_A - R_N}{V_{muzzle}} = \frac{\theta_1 + \theta_2 + \theta_3}{\omega} \tag{7}$$

$$\omega = \frac{2\pi n}{60} \tag{8}$$

In Equations (7) and (8), R_A represents the radius at (point A)'s position; R_N denotes the radius at (point N)'s position; V_{muzzle} indicates the oil injection nozzle velocity; ω signifies the angular velocity of the oil scoop, with units of rad/s; n stands for the rotational speed of the oil scoop, with units of rpm.

Under these conditions, if $\Delta R = R_A - R_N$, the relationship between the nozzle velocity and oil scoop rotational speed can be expressed as:

$$\frac{n}{V_{muzzle}} = \frac{60}{\Delta R \cdot N} \tag{9}$$

2.2. Motion Analysis of Lubricating Oil on Inner and Outer Surfaces of Oil Scoop

When the lubricating oil jet collides with the scoop tip, the injection velocity of the oil is much lower than the linear velocity of the scoop. At the moment of contact, the jet can be considered stationary. Subsequently, as the scoop rotates at high speed, the "cut" lubricating oil, under the influence of the centrifugal force, completely adheres to the inner surface of the scoop and flows toward the inlet of the oil delivery channel.

Under these conditions, assuming the inner wall of the scoop is straight and the cut lubricating oil jet completely adheres to the inner surface, the velocity analysis of a lubricating oil micro-element during flow along the inner surface is shown in Figure 6. Here, V_1 represents the absolute velocity of the micro-element, while V_2 denotes the convective velocity relative to the coordinate system, which is equal in magnitude but opposite in direction to the linear velocity of the main shaft rotation. The absolute velocity and convective velocity of the micro-element are each resolved into two components: one parallel to the inner surface direction and one normal to it. The figure shows that the micro-element's velocity parallel to the inner surface is $V = V_1 \cos\theta_1 + V_2 \cos\theta_2$. This leads to the conclusion that the flow velocity of the lubricating oil along the inner surface after being cut is proportional to both the linear velocity of the main shaft rotation and the nozzle injection velocity.

Figure 7 shows the force analysis diagram of the lubricating oil micro-element at representative positions 1, 2, and 3 on the inner surface. Assuming the inner surface is flat within these three positions. O is the main shaft axis and θ is the angle between the

inner surface and horizontal line. The centrifugal force direction is opposite but equal in magnitude to the centripetal force. The centrifugal forces at the three positions are F_1, F_2 and F_3, each resolved into y-direction (normal to inner surface) and x-direction (parallel to inner surface) components.

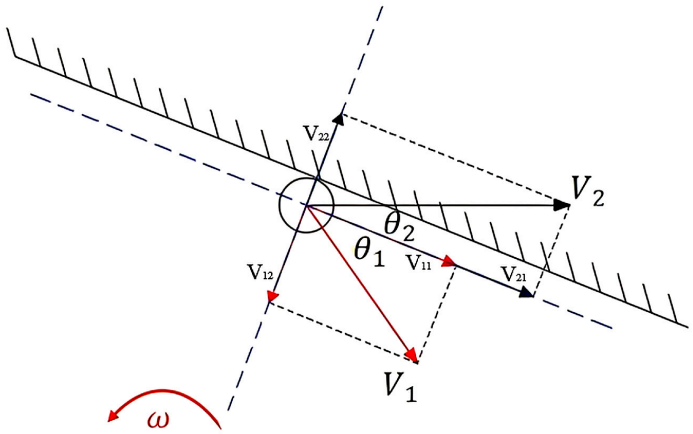


Figure 6. Velocity analysis of micro-elements of lubricating oil flowing on the inner surface of oil scoop.

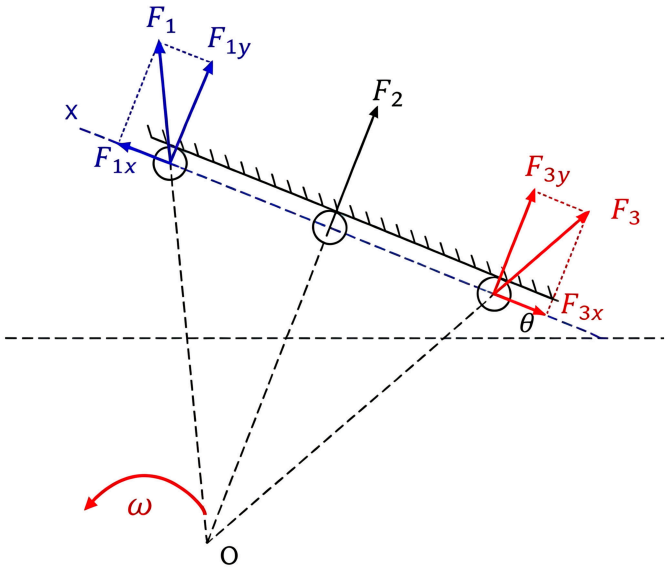


Figure 7. Force analysis of the micro-elements of lubricating oil flowing on the inner surface of oil scoop.

When the micro-element is at position 1, the centrifugal component F_{1x} opposes the actual flow direction, slowing the lubricant velocity. When the micro-element is at position 2, the centrifugal force acts perpendicular to the inner surface, with no x-direction effect on velocity. When the micro-element is at position 3, the centrifugal component F_{1x} aligns with the flow direction, accelerating the lubricant.

If the lubricant reaches position 2 without spillage, the centrifugal component will enhance flow beyond this equilibrium point.

Considering the lubricant's high viscosity, sliding friction in the y-direction must be accounted for. Both the centrifugal component and sliding friction reduce flow velocity. To prevent collected oil from spilling, Equation (10) must be satisfied.

$$\frac{1}{2}mV_{oil}^2 - F_{cen}l\sin\theta + \mu\cos\theta > 0 \tag{10}$$

In Equation (10), F_{cen} represents the centrifugal force acting on the lubricating oil micro-element.

Since the gravity of the oil micro-element is not considered, when the jet collides with the outer surface of the scoop before being cut by the scoop, the flow principle of the lubricating oil on the outer surface of the scoop and the factors affecting its flow velocity are the same as those when the lubricating oil flows on the inner surface of the scoop.

2.3. Preliminary Design of the Outer Surface Curve of Oil Scoop

The outer surface curve of the oil scoop is determined based on the geometric relationship between the vertical nozzle and the scoop. According to the aforementioned analysis results, the radial oil scoop in this bearing lubrication device serves two functions: first, cutting the jet stream; second, when the jet contacts the outer surface before being cut, guiding the lubricant flow. Therefore, the oil scoop is divided into two parts for design: Scoop I is responsible for jet cutting, while Scoop II adjusts the number of blades and guides lubricant flow along the outer surface. Figure 8 shows the geometric relationship of the preliminarily designed outer surface curve of the radial oil scoop for the subsequent structural design.

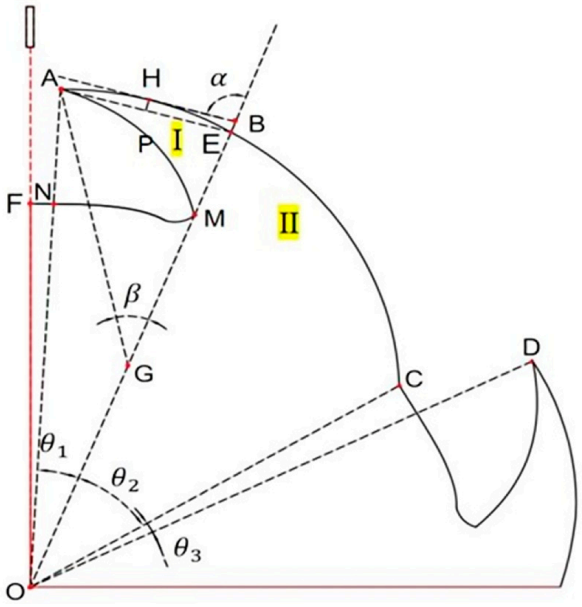


Figure 8. Geometric relation of the preliminarily designed outer surface curve of the radial oil scoop for the subsequent structural design.

3. CFD Investigations on Structural Optimization of Oil Scoop

3.1. Calculation Model

A 3D model of the oil scoop in the under-race lubrication device was established in SolidWorks 2021, and the corresponding fluid domain was extracted using DesignModeler in ANSYS 2022 R1. Because the 3D model requires a large number of cells and a small time step, the computational cost is high, which makes parametric studies under different operating conditions and structural variables impractical. Previous studies [28,29] showed that the 2D model provides capture-efficiency trends consistent with those of the 3D model, so the 2D model was adopted here to improve computational efficiency. As shown in Figure 9, the computational fluid domain was divided into three regions: two stationary regions (red and white) and one rotating region (green).

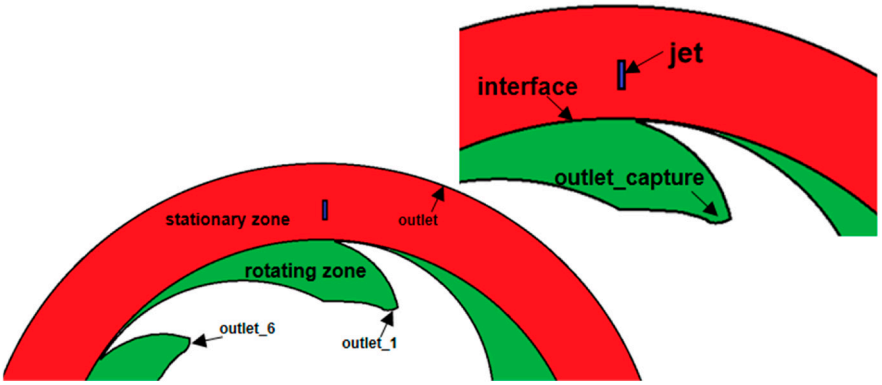


Figure 9. 2D simulation calculation model of radial oil scoop.

According to the working principle of the radial oil scoop, its performance is evaluated by the oil capture efficiency. The oil capture efficiency is defined as the ratio of the lubricating-oil mass flow rate at the oil outlet (outlet_capture) to that at the jet inlet (inlet), as expressed in Equation (11).

$$\eta = \sum_{i=1}^{N} \frac{\dot{M}_{capture} \Delta t_i}{\dot{M}_{inlet} \Delta t_i} \tag{11}$$

In Equation (11), the variables represent the total number of calculated time steps, the lubricating-oil mass flow rate at the oil outlet, and the lubricating-oil mass flow rate at the jet inlet.

To evaluate mesh sensitivity, three mesh sizes of 0.2 mm, 0.3 mm, and 0.4 mm were tested under a jet speed of 20 m/s and a rotational speed of 9000 rpm. As listed in Table 1, the predicted oil capture efficiency increased from 62.1% to 66.3% as the mesh became coarser. The corresponding mesh numbers were 105,873, 47,291, and 27,462, respectively. The finer mesh was able to resolve smaller oil structures and splashing behavior more clearly, whereas the coarser meshes tended to miss small droplets and thus overpredict capture efficiency.

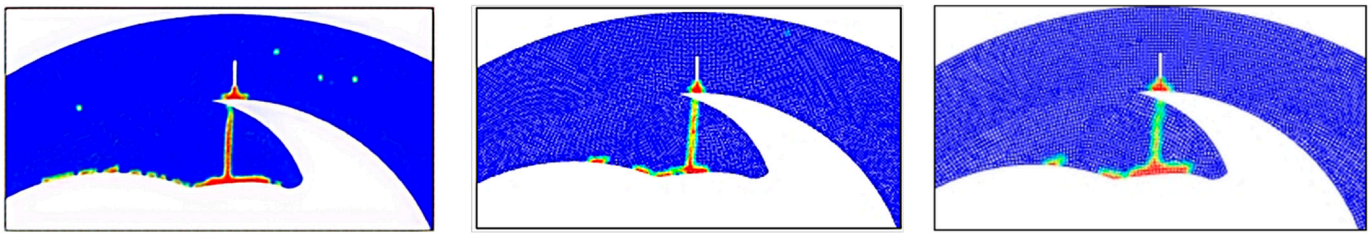
Table 1. Simulation results for different mesh sizes.

Mesh Size (mm)	Mesh Quantity	Oil Capture Efficiency (%)	Deviance (%)
0.2	105,873	62.1	0
0.3	47,291	64.7	+2.6
0.4	27,462	66.3	+4.2

Figure 10 further compares the instantaneous flow-field distributions obtained with the three mesh sizes, showing that the finer mesh captures droplet morphology and splash details more clearly. Therefore, the 0.2 mm mesh, which is the finest mesh considered in the present study, was conservatively selected for subsequent simulations to reduce the risk of overpredicting oil capture efficiency and to provide more reliable interface resolution for comparative analysis.

Because the oil capture process involves immiscible oil–air flow with a distinct interface, the Volume of Fluid (VOF) model was adopted. The simulations were performed using a pressure-based transient solver. The nozzle was defined as a velocity inlet, while the drainage-channel outlets and splash outlet were set as pressure outlets. To represent the actual motion of the scoop, the rotating region shown in Figure 9 was treated as a rotating zone and connected to the stationary regions through interfaces using a sliding-mesh approach. The lubricant properties used in the simulations were density 969.6 kg/m^3 and dynamic viscosity 0.01123 Pa·s. To account for turbulence in the oil–air flow field, the

RNG k-epsilon turbulence model was adopted within the RANS framework. Compared with the standard k-epsilon model, the RNG k-epsilon model is better suited to rapidly strained and rotational flows, and is therefore more appropriate for the present oil capture process involving strong velocity gradients and centrifugal effects. Standard wall treatment was applied near the wall boundaries. Pressure–velocity coupling was achieved using the SIMPLE algorithm, and the residual convergence criterion was set to 1×10^{-6}.



(**a**) (**b**) (**c**)

Figure 10. Instantaneous flow-field comparison for three mesh sizes under the same operating condition (jet speed 20 m/s, rotational speed 9000 rpm) ((**a**) 0.2 mm; (**b**) 0.3 mm; (**c**) 0.4 mm).

In the present simulations, the lubricant jet was treated as a continuous inlet flow, while secondary breakup, atomization, and detailed aerodynamic deflection were neglected. This assumption is reasonable for the tested operating range and the short interaction distance between nozzle and scoop, where the primary oil capture process is dominated by jet cutting and surface-guided transport. Nevertheless, under more extreme rotational speeds or stronger air entrainment, these effects may increase oil dispersion and splash loss, so the current model may slightly overestimate the capture efficiency. This limitation should be considered when extending the present method to broader operating conditions. Accordingly, the present simulations should be interpreted as a mechanism-oriented and trend-oriented approximation of the oil capture process within the investigated operating range.

The present model and validation are limited to the investigated operating range. For substantially higher rotational speeds, stronger splash and oil–air interaction may lead to more pronounced three-dimensional effects.

3.2. Analysis of Influencing Factors on Oil Capture Efficiency of Oil Scoop

Based on the analysis of the oil capture mechanism, it can be preliminarily inferred that the oil jet velocity, rotational speed, scoop adjustment angle, and blade number all influence oil capture efficiency. Because factors such as oil jet velocity are external parameters, the scoop adjustment angle and blade number were selected as the main variables for the simulation analysis to obtain preliminary optimization results. The results are shown in Figure 11.

For different blade adjustment angles, blade models with adjustment angles ranging from 90° to 115° in increments of 5° (shown in Figure 12) were simulated at four rotational speeds under a jet speed of 20 m/s. This range was selected according to the structural layout and feasible design space of the scoop. In the present study, 90° was taken as the lower bound for the investigated range, while smaller angles were not further considered within the current design constraints. The corresponding oil capture efficiencies are presented in Figure 11a. As the blade adjustment angle increases, the oil capture efficiency decreases at all four rotational speeds. At higher rotational speeds, the oil capture efficiency of the scoop is consistently higher than that at lower rotational speeds. When the blade adjustment angle is less than or equal to 100°, the lubricant flowing along the outer surface of Blade II enters the drainage groove directly without forming a plume that causes splashing. Therefore, the oil capture efficiency is higher when the blade adjustment angle is below 100°.

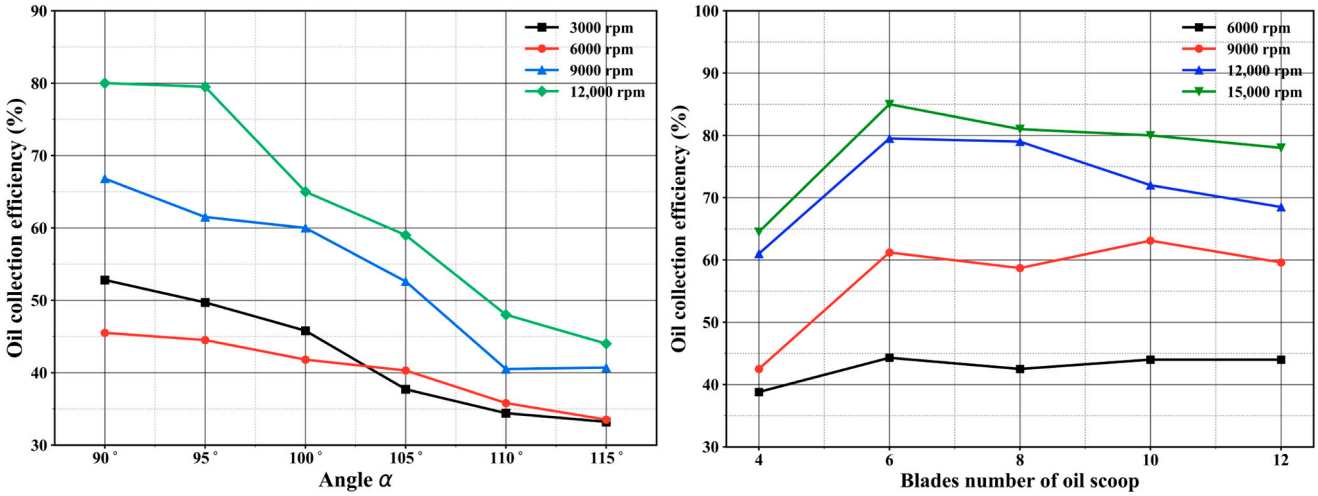


Figure 11. Oil capture efficiency of oil scoop under different factors. ((**a**) Blade adjustment angle α at different rotational speeds; (**b**) number of blades at different rotational speeds).

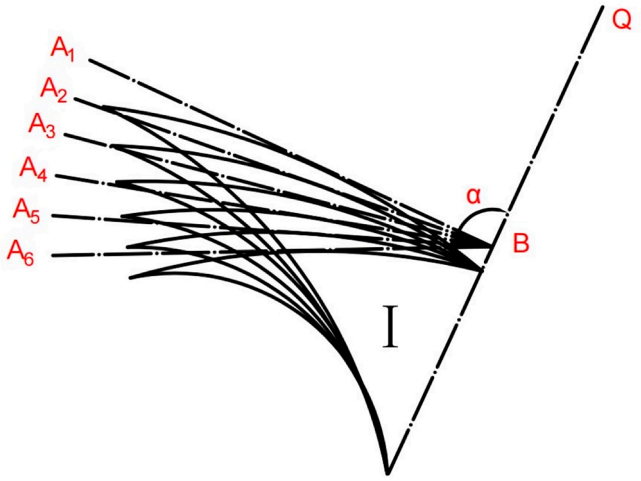


Figure 12. Blade I at different adjustment angles.

For different blade numbers, because the oil collecting structure supplies oil on both sides, the total number of blades should be 2n to ensure uniform lubricant distribution on both sides. Owing to geometric constraints, the upper limit of blade number was set to 12. Simulations were performed at four rotational speeds for blade numbers of 4, 6, 8, 10, and 12 under a jet speed of 20 m/s. The resulting oil capture efficiencies are shown in Figure 11b. When the scoop has six blades, the oil capture efficiency is significantly higher than that of the four-blade configuration.

However, when the number of blades exceeds six, the oil capture efficiency no longer improves significantly, and even decreases at higher rotational speeds. This is because the blade number reflects a balance between jet interception frequency and internal flow passage availability. Too few blades cannot intercept the incoming oil jet effectively, whereas too many blades reduce the effective flow space and intensify flow interference. Therefore, considering both manufacturing cost and oil capture performance, the six-blade scoop is a more suitable choice.

3.3. Flow Field Visualization Analysis for Discussing Oil Loss Mechanism

Based on the selected adjustment angle and blade number, the mechanism of lubricant loss during scoop operation is analyzed using the case shown in Figure 13 as an example.

Figure 13 illustrates the oil capture process and the flow state on the outer scoop surface at a rotational speed of 12,000 rpm and a jet speed of 20 m/s. The analytical model is intended to provide a mechanistic interpretation of the capture and spillage process, while the CFD results offer flow-field evidence supporting the identified loss pathways. In this way, the theoretical and numerical analyses are used in a complementary manner to explain the observed efficiency variations.

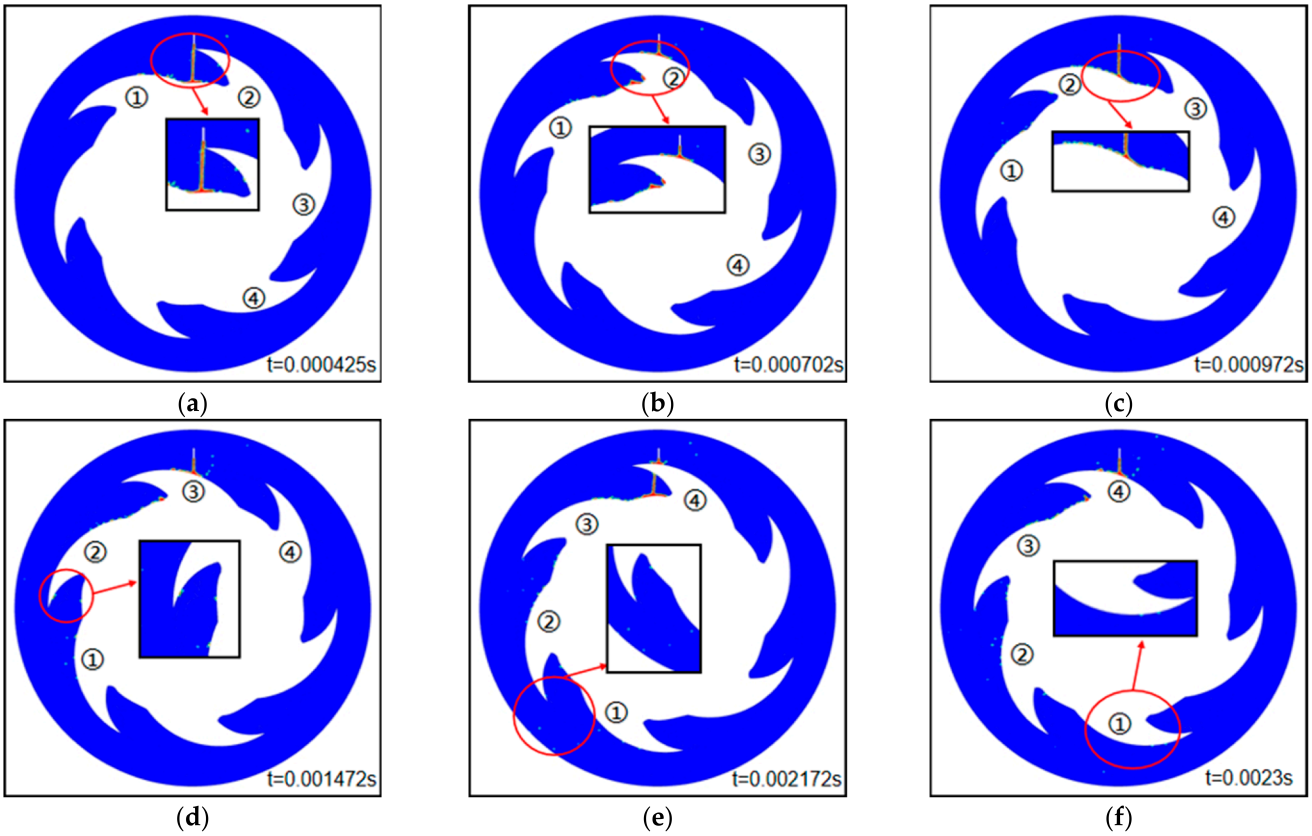


Figure 13. The working process of primary oil capture at speed 12,000 rpm. ((**a**) t = 0.000425 s; (**b**) t = 0.000702 s; (**c**) t = 0.000972 s; (**d**) t = 0.001472 s; (**e**) t = 0.002172; (**f**) t = 0.00230 s).

As shown in Figure 13, at the beginning of the oil capture process, the jet cut by the scoop flows into the corresponding drainage channel under inertial force. Part of the cut jet may contact the outer surface of the scoop, where the lubricating oil divides into two portions: one flows toward the scoop leading edge, while the other continues toward the drainage channel. The former may be ejected from the drainage channel due to excessive velocity, spilling out of the capture area along the inner surface, while the latter flows through the drainage channel into the oil delivery section. Subsequently, when the jet can no longer provide propulsion for oil on the outer surface, the oil flow velocity gradually decreases to zero under viscous friction and centrifugal forces, eventually splashing outward due to centrifugal action, resulting in oil loss.

Analysis of various factors affecting capture efficiency reveals two primary causes of oil loss:

(1) When the operating condition exceeds a certain threshold, the jet contacts the outer surface of the scoop before the next cutting event occurs, causing a significant amount of lubricant to flow along the outer surface. Under the combined effects of jet momentum, rotational motion, and surface interaction, part of this lubricant is eventually ejected from the capture area, resulting in oil loss and reduced oil capture efficiency.

(2) After the oil flow contacts the outer surface of the scoop, one portion of the oil flows under the influence of viscous friction and after losing the propulsion force from the jet it will move toward the drainage channel with its velocity gradually decreasing to zero. This portion of oil flow will then be ejected onto the inner surface of the scoop by centrifugal force, subsequently flowing out of the capture area, resulting in lubricating oil loss and decreased oil capture efficiency.

The visualization results indicate that outer-surface backflow followed by centrifugal ejection is a major loss pathway under the investigated conditions. Based on this observation, the subsequent structural optimization was designed to redirect lubricant into the drainage groove before splash loss becomes dominant.

3.4. Structure Optimization Analysis of Oil Scoop

Based on the above investigations, the preliminary scoop design was structurally optimized. To reduce the contact time between the oil jet and the outer blade surface, while improving the capture of lubricant flowing along the outer surface, a disconnected drainage groove C with a width of 1.5 mm was added at the midpoint of the outer blade surface, as shown in Figure 14a. This modification divides the original blade into two mini-blades, A and B, allowing more lubricant on the outer surface to enter the next stage before splashing occurs and thereby improving the oil capture efficiency.

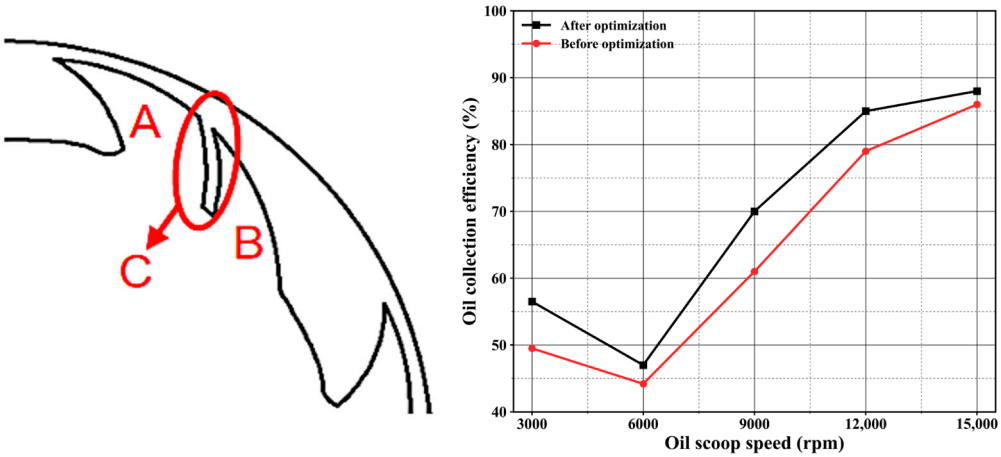


Figure 14. Optimized oil scoop structure and comparison of the simulated oil capture efficiencies before and after optimization: (**a**) optimized blade structure; (**b**) efficiency comparison.

Figure 14b compares the oil capture efficiencies before and after optimization under different rotational speeds. The optimized design increases the oil capture efficiency by about 5–12%, while preserving the same overall trend with rotational speed, indicating that the proposed structural modification is effective in improving scoop performance.

From an engineering perspective, the 5–12% increase in capture efficiency means that a larger fraction of the supplied lubricant can be guided into the under-race lubrication path rather than being lost by splash. This is expected to improve the continuity of oil supply to the bearing, reduce the risk of local starvation, and strengthen cooling and oil-film formation under high-speed conditions. Therefore, the optimized scoop design has practical value for enhancing lubrication reliability in aerospace transmission systems.

Based on the above results, further optimization of the height difference and the number of mini-blades was carried out as follows:

Geometric model of the different height difference of small blades represented in Figure 15a. The center of the spindle axis is taken as the center of the circle and the distance

between the center of the circle and point A is taken as the radius to determine the circle with radius r_1, and the arc $\widehat{AR_1}$ is shown in the figure. The circle with radius difference of 2 mm is made with the axis as the center of the circle, and the arcs $\widehat{BR_2}$, $\widehat{CR_3}$ and $\widehat{DR_4}$ between the inner surface of the blade and the outer surface of the drainage groove C are intercepted. The arc $\widehat{OA}$ was rotated to the points B, C and D with the point O as the center of the circle to obtain the new small blades 2, 3 and 4 respectively. In order to study the influence of the height difference between the small blades on the oil collecting efficiency of the optimized oil scoop, the simulation calculation is carried out by the oil jet speed of 20 m/s. The oil collecting efficiencies of oil scoop are obtained with the height difference between the small blades under different rotation speeds are shown in Figure 15b.

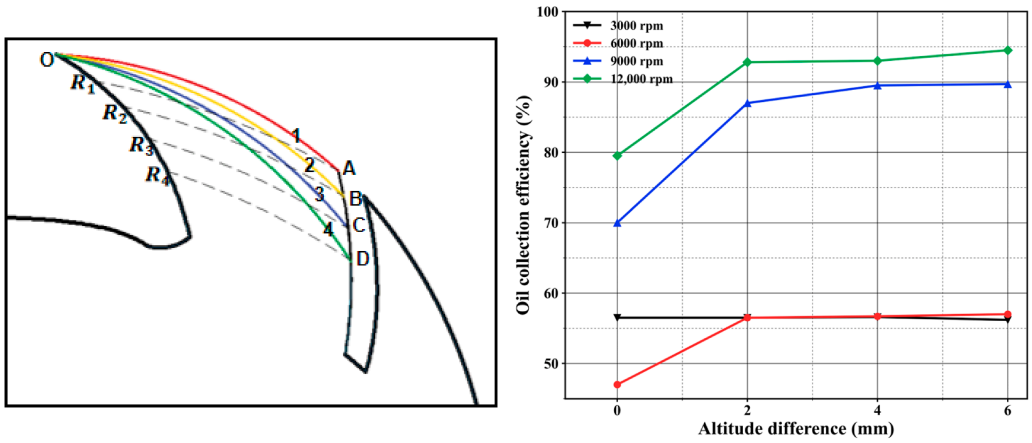


Figure 15. Geometric models with different mini-blade height differences and the corresponding oil capture efficiencies at different rotational speeds. ((**a**) Geometric models; (**b**) efficiency comparison).

When there is no height difference between the blades, a plume forms when the jet flows into drainage groove C, which causes the lubricant to splash out of the oil capture area and results in oil loss. When a height difference exists between Blades A and B, plume formation can be avoided. This allows more lubricant on the outer blade surface to flow into drainage groove C before splashing occurs, thereby reducing oil loss and greatly improving the oil capture efficiency. However, as the height difference continues to increase, there is a limit to the amount of lubricant that can flow from the outer surface into drainage groove C. Consequently, the incremental improvement in oil capture efficiency becomes less pronounced at larger height differences.

Increasing the number of mini-blades increases the number of drainage-groove inlets, thereby providing more opportunities for lubricant to enter the drainage groove. The original blade was subdivided at intervals of 1/2, 1/3, and 1/4 of its length to obtain configurations with two, three, and four mini-blades, as shown in Figure 16. The height difference between adjacent mini-blades was set to 1 mm. To investigate the influence of mini-blade number on the oil capture efficiency after optimization, simulations were performed at a jet speed of 20 m/s, and the resulting variation in oil capture efficiency with mini-blade number at different rotational speeds is shown in Figure 17.

From Figure 17, at a rotational speed of 6000 rpm, the largest increase in oil capture efficiency occurs when the number of mini-blades is increased to three. However, at the other three rotational speeds, the largest increase in oil capture efficiency is obtained when the number of mini-blades is increased to two. In addition, after the initial improvement in efficiency, the influence of further increasing the number of mini-blades gradually diminishes at all four rotational speeds.

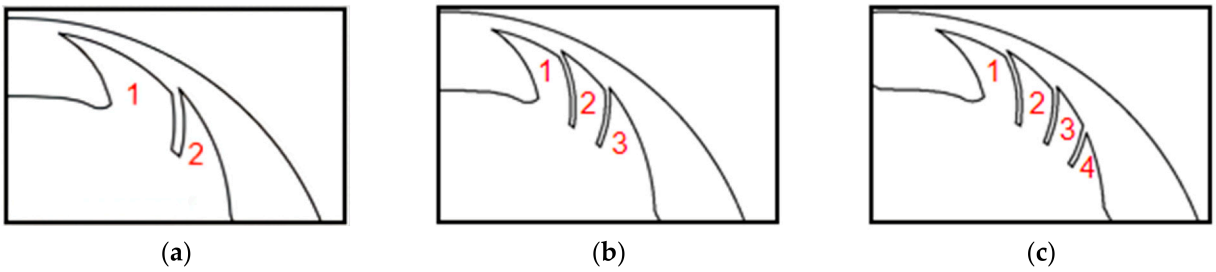


Figure 16. Geometrical model of different small blade numbers. ((**a**) Two mini-blades; (**b**) three mini-blades; (**c**) four mini-blades).

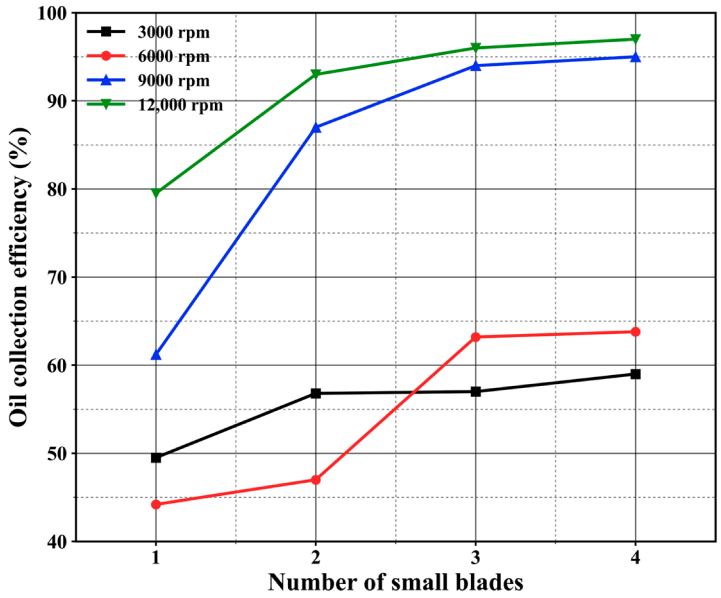


Figure 17. Oil capture efficiencies with different small blade numbers and different rotation speeds.

Compared with the conventional scoop, the optimized design introduces additional geometric details, such as subdivided blades and an added drainage groove, which may slightly increase machining complexity. However, the optimized design does not require a fundamentally different manufacturing route and remains compatible with conventional precision machining methods. The present study focuses on mechanism-guided sequential optimization to identify effective structural improvements.

4. Validation of the Simulation Method of Oil Scoop

An experimental platform for evaluating the oil capture performance of high-speed bearings with under-race lubrication was established to validate the feasibility of the simulation methods mentioned earlier. The test platform primarily consists of four modular components: the lubrication system, mechanical system, measurement and control system, and test bench frame. A schematic diagram of the test bench logic and test platform are shown in Figures 18 and 19, respectively.

The test bench has the following features. First, it allows independent adjustment of the main-shaft rotational speed and nozzle jet velocity. Second, it enables measurement of both the mass of lubricant collected by the scoop and the mass not captured. Third, its modular design facilitates replacement of test components.

To facilitate measurement of the lubricant mass collected by the scoop, the oil capture structure in the bearing lubrication device was modified. The redesigned capture structure primarily consists of left and right oil-baffle walls, the oil scoop, and an added capture chamber. The capture chamber was specifically designed to hold industrial oil-absorbent

paper for convenient measurement of the collected lubricant mass. Because the oil capture efficiency is primarily influenced by the outer surface curve of the oil scoop, aside from scoop number, rotational speed, and injection velocity, a 1.5× scaled-up version of the simulation model was used for testing to improve measurement accuracy. Therefore, the scaled experiment in the present study was primarily intended for comparative trend validation of the capture behavior, rather than strict full-scale dynamic-similarity reproduction.

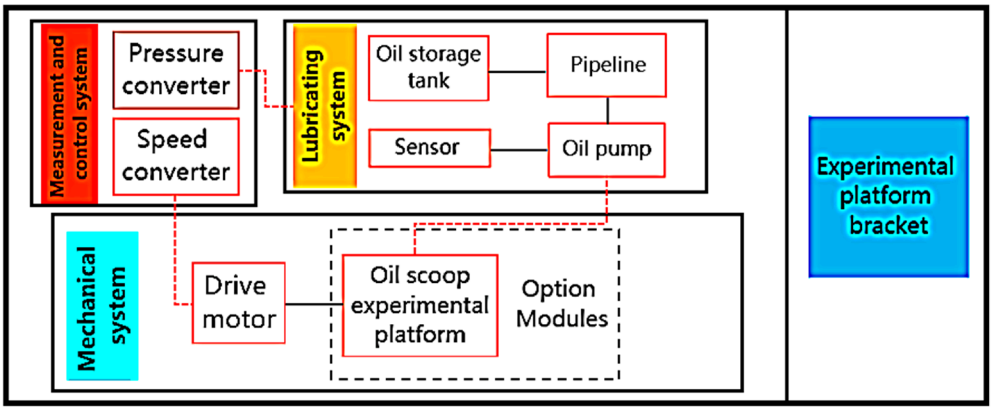


Figure 18. Logical schematic diagram of oil scoop oil experimental platform.

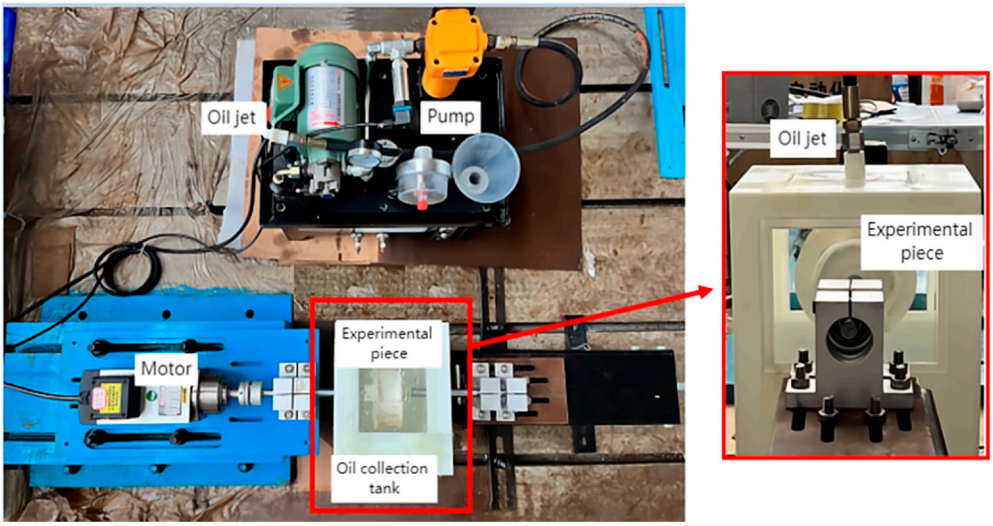


Figure 19. Experimental platform of oil scoop.

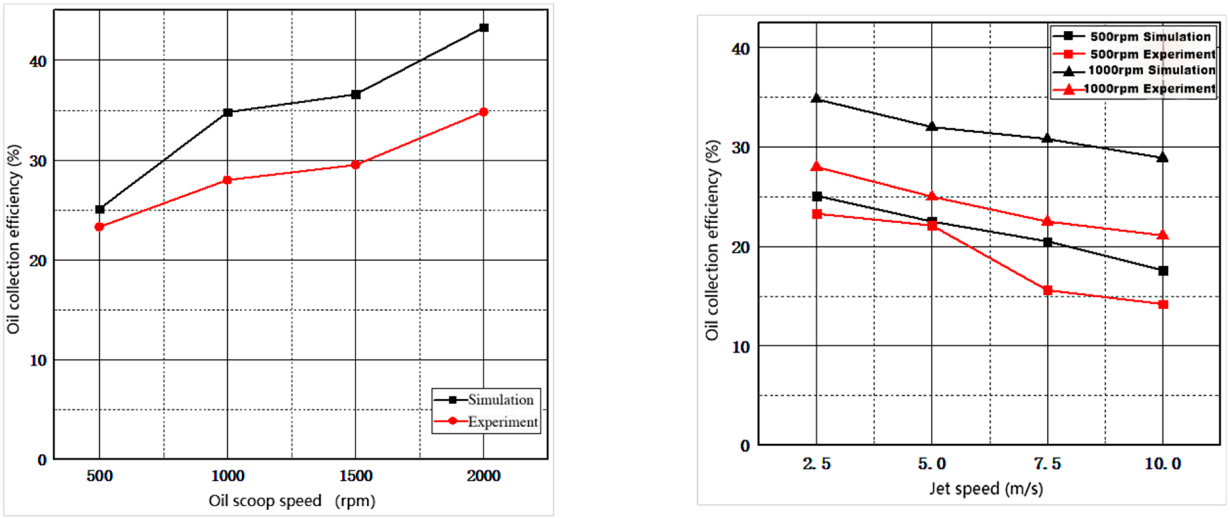
To evaluate capture efficiency under different injection velocities, monitoring of nozzle jet velocity was required. However, due to experimental limitations preventing direct velocity measurement, the jet velocity was adjusted by varying the oil supply pressure in the lubrication system. The main shaft speed was controlled using a frequency converter. In addition to shaft speed, the test required varying nozzle jet velocities to establish the corresponding relationship with scoop performance. Preliminary testing was conducted to determine four specific oil supply pressures corresponding to target injection velocities, as summarized in Table 2.

The test specimen used an oil scoop with a 95° adjustment angle. Following the simulation method described earlier, experiments were conducted by varying rotational speed and injection velocity to measure the oil capture efficiency of the scoop and compare the results with the simulated values. Specifically, the variation in oil capture efficiency with rotational speed was obtained at a fixed jet speed of 5 m/s, and the variation in oil

capture efficiency with jet speed was obtained at fixed rotational speeds of 500 rpm and 1000 rpm, as shown in Figure 20.

Table 2. Corresponding relation between oil jet speed and oil supply pressure of the lubrication system.

Oil Jet Speed	Oil Supply Pressure
2.5 m/s	0.05 Mpa
5 m/s	0.12 Mpa
7.5 m/s	0.16 Mpa
10 m/s	0.24 Mpa



(**a**) (**b**)

Figure 20. Comparison between experimental and simulated oil capture efficiencies under different operating conditions. ((**a**) Effect of rotational speed at a fixed jet speed; (**b**) effect of jet speed at fixed rotational speeds).

As shown in Figure 20a, the oil capture efficiency increases with rotational speed at a fixed jet speed. As shown in Figure 20b, the oil capture efficiency decreases with increasing jet speed at a fixed rotational speed.

Under the investigated operating conditions, the experimental and simulated results show the same overall trends: the oil capture efficiency increases with rotational speed and decreases with oil jet speed. In general, the experimental values are slightly lower than the simulated ones, indicating that the numerical model can reasonably capture the variation in scoop performance under different operating conditions. The present validation is therefore mainly intended to support the observed performance trends and the comparative effectiveness of the proposed structural optimization.

5. Conclusions

The lubricant flow mechanism in the oil capture section of radial under-race lubrication was analyzed, and the main factors affecting capture efficiency were identified. Using CFD methods, numerical simulations of the oil capture process were conducted on this basis, followed by structural optimization of the scoop and experimental validation of the simulation trends. The study provides a useful reference for the design of the oil capture section in radial under-race lubrication systems. The main conclusions are as follows:

(1) The oil capture mechanism of the radial under-race oil scoop was analyzed theoretically, showing that the jet velocity, rotational speed, scoop geometry, and blade arrangement jointly determine the oil capture behavior and splash loss.

(2) CFD simulations revealed that excessive oil loss mainly occurs when lubricant flows along the outer blade surface and is subsequently splashed out by centrifugal action. Based on this mechanism, an optimized scoop with an additional drainage groove and subdivided blades was proposed, increasing oil capture efficiency by about 5–12%.

(3) Experimental results showed the same variation trends as the simulations under different rotational speeds and jet velocities, supporting the applicability of the numerical method for capturing the observed performance trends. The optimized design is expected to improve lubricant delivery continuity and lubrication reliability for high-speed aerospace transmission bearings.

Author Contributions: Conceptualization, X.H.; methodology, K.D. and B.H.; software, K.D. and B.H.; validation, K.D. and B.H.; writing—original draft preparation, K.D.; writing—review and editing, X.H. and K.D.; visualization, K.D.; project administration, X.H. All authors have read and agreed to the published version of the manuscript.

Funding: This research received no external funding.

Institutional Review Board Statement: Not applicable.

Informed Consent Statement: Not applicable.

Data Availability Statement: All data generated or analyzed during this study are included in this article.

Acknowledgments: The authors would like to acknowledge the guidance and review provided by the corresponding author, Xiaozhou Hu. We also extend our gratitude to Kang Duan for his contribution to the simulation work, experimental validation, and data processing.

Conflicts of Interest: The authors declare no conflicts of interest.

References

1. Pinel, S.I.; Signer, H.R.; Zaretsky, E.V. Comparison Between Oil-Mist and Oil-Jet Lubrication of High-Speed, Small-Bore, Angular-Contact Ball Bearings. *Tribol. Trans.* **2001**, *44*, 327–338. [CrossRef]
2. Nakamura, S.; Kakino, Y.; Urano, K.; Yoneyama, H. An Analysis and a Performance Evaluation of the Under-Race Lubrication Spindle at a High Speed Rotation. *J. Jpn. Soc. Precis. Eng.* **1994**, *60*, 1485–1489. [CrossRef]
3. Adeniyi, A.; Morvan, H.; Simmons, K. A Computational Fluid Dynamics Simulation of Oil–Air Flow Between the Cage and Inner Race of an Aeroengine Bearing. *ASME J. Eng. Gas Turbines Power* **2017**, *139*, 012506. [CrossRef]
4. Bao, H.; Hou, X.; Lu, F. Analysis of Oil-Air Two-Phase Flow Characteristics inside a Ball Bearing with Under-Race Lubrication. *Processes* **2020**, *8*, 1223. [CrossRef]
5. Bao, H.; Hou, X.; Tang, X.; Lu, F. Analysis of temperature field and convection heat transfer of oil-air two-phase flow for ball bearing with under-race lubrication. *Ind. Lubr. Tribol.* **2021**, *73*, 817–821. [CrossRef]
6. Jiang, L.; Lyu, Y.; Gao, W.; Zhu, P.; Liu, Z. Numerical investigation of the oil–air distribution inside ball bearings with under-race lubrication. *Proc. Inst. Mech. Eng. Part J J. Eng. Tribol.* **2022**, *236*, 499–513.
7. Lyu, Y.; Li, Y.; Li, C.; Jiang, L.; Liu, Z. Oil-Air Distribution Prediction Inside Ball Bearing with Under-Race Lubrication Based on Numerical Simulation. *Appl. Sci.* **2024**, *14*, 3770. [CrossRef]
8. Gao, W.; Li, C.; Li, Y.; Liu, Z.; Lyu, Y. Oil–Air Two-Phase Flow Distribution Characteristics inside Cylindrical Roller Bearing with Under-Race Lubrication. *Lubricants* **2024**, *12*, 133. [CrossRef]
9. Gao, W.; Li, Y.; Li, C.; Xu, Y.; Liu, Z. Numerical prediction of drag force on spherical elements inside high-speed ball bearing with under-race lubrication. *Mech. Syst. Signal Process.* **2025**, *224*, 112024. [CrossRef]
10. Kenneth, L.F.; Herbert, F.D.; Rodney, H. Methods and Apparatus for Supplying Oil to Bearing Assemblies. U.S. Patent 6,409,464, 25 June 2002.
11. Kenneth, L.F. Bi-Directional Oil Scoop for Bearing Lubrication. U.S. Patent 6,682,222, 27 January 2004.
12. Joseph, D.; James, B. Lubricant Scoop. U.S. Patent 10,662,812, 26 May 2020.
13. Stephen, T.M. Liquid-Capturing Shaft. U.S. Patent 10,113,429, 30 October 2018.
14. Paleo, C.P.; Simmons, K.; Prabhakar, A.; Chandra, B. Assessment of the Oil Scoop Capture Efficiency in High Speed Rotors. *J. Eng. Gas Turbines Power* **2019**, *141*, 012401.

15. Lyu, Y.; Jiang, L.; Liu, Z.; Hu, J. Simulation and Analysis of Oil Scoop Capture Efficiency. In Proceedings of the ASME Turbo Expo 2018: Turbo Machinery Technical Conference and Exposition, Oslo, Norway, 11–15 June 2018; p. V001T01A022.
16. Jiang, L.; Liu, Z.; Lyu, Y.; Zhu, P. Numerical Study on Flow Characteristics of Liquid Jet in Airflows. In Proceedings of the ASME Turbo Expo 2019: Turbomachinery Technical Conference and Exposition, Phoenix, AZ, USA, 17–21 June 2019; p. V001T01A018.
17. Jiang, L.; Liu, Z.; Lyu, Y.; Qin, J. Numerical simulation on the oil capture performance of the oil scoop in the under-race lubrication system. *J. Aerosp. Eng. Part G* **2021**, *235*, 2258–2273. [CrossRef]
18. Jiang, L.; Lyu, Y.; Li, Y.; Liu, Y.; Hou, Y.; Liu, Z. Numerical and Experimental Investigations to Assess the Impact of an Oil Jet Nozzle with Double Orifices on the Oil Capture Performance of a Radial Oil Scoop. *Aerospace* **2023**, *10*, 1015. [CrossRef]
19. Jiang, L.; Liu, Z.; Huang, W.; Lyu, Y.; Li, Y.; Gao, W.; Liu, Y. Influence and optimization of dual-orifice jet nozzles on oil capture performance of under-race lubrication with a radial oil scoop for high-speed bearings in aero-engine. *Phys. Fluids* **2024**, *36*, 20. [CrossRef]
20. Hou, Y.; Jiang, L.; Lyu, Y.; Gao, W.; Liu, Y.; Liu, Z. Optimization and influence of oil supply parameters on oil capture characteristics of radial oil scoop for high-speed bearings. *Tribol. Int.* **2024**, *199*, 110028. [CrossRef]
21. Jiang, L.; Lyu, Y.; Liu, Z. Investigation on two-phase flow characteristics and oil capture performance of axial oil scoop in aero-engine. *Case Stud. Therm. Eng.* **2023**, *49*, 103259. [CrossRef]
22. Zhang, C.; Jiang, L.; Lyu, Y.; Gao, W.; Liu, Y.; Liu, Z. Analysis of oil capture characteristics and global sensitivity of radial oil blades with different blade radius differences for high-speed bearings. *Simul. Model. Pract. Theory* **2025**, *139*, 103057. [CrossRef]
23. Kruisbrink, A.; Cageao, P.P.; Morvan, H.P.; Simmons, K. Operating under jet splashing conditions can increase the capture efficiency of blades. *Int. J. Heat Fluid Flow* **2019**, *76*, 296–308. [CrossRef]
24. Jonathan, E.; John, H.; Arun, K. Curved Blade Oil Scoop. U.S. Patent 7,244,096, 17 July 2007.
25. Qin, J.; Guo, H.; Jiang, H.; Wang, F.; Man, W.; Lyu, Y. Novel design and simulation of curved blade oil scoop with high oil capture efficiency. *Chin. J. Aeronaut.* **2021**, *34*, 94–103. [CrossRef]
26. Milojević, S.; Savić, S.; Mitrović, S.; Marić, D.; Krstić, B.; Stojanović, B.; Popović, V. Solving the Problem of Friction and Wear in Auxiliary Devices of Internal Combustion Engines on the Example of Reciprocating Air Compressor for Vehicles. *Teh. Vjesn.* **2023**, *30*, 122–130. [CrossRef]
27. Gajević, S.; Marković, A.; Milojević, S.; Ašonja, A.; Ivanović, L.; Stojanović, B. Multi-Objective Optimization of Tribological Characteristics for Aluminum Composite Using Taguchi Grey and TOPSIS Approaches. *Lubricants* **2024**, *12*, 171. [CrossRef]
28. Korsukova, E.; Kruisbrink, A.; Morvan, H.; Paleo Cageao, P.; Simmons, K. Oil Scoop Simulation and Analysis Using CFD and SPH. In Proceedings of the ASME Turbo Expo 2016: Turbomachinery Technical Conference and Exposition, Seoul, Republic of Korea, 13–17 June 2016; p. V07BT31A027.
29. Korsukova, E.; Morvan, H. Computational Fluid Dynamics Study of Oil Behavior in a Scoop and Factors Affecting Scoop Capture Efficiency. *J. Eng. Gas Turbines Power Trans. ASME* **2020**, *142*, 051008. [CrossRef]

Disclaimer/Publisher's Note: The statements, opinions and data contained in all publications are solely those of the individual author(s) and contributor(s) and not of MDPI and/or the editor(s). MDPI and/or the editor(s) disclaim responsibility for any injury to people or property resulting from any ideas, methods, instructions or products referred to in the content.